TECHNICAL ARTICLE

Nonlinear 3PB and 4PB Flexural Behavior and Softening Localization for Epoxy Resin E 863 Using Digital Image Correlation Technique

M.Y. Fard, A. Chattopadhyay, and Y. Liu

Department of Mechanical and Aerospace Engineering, School for Engineering of Matter, Transport and Energy, Arizona State University, Tempe, AZ

Keywords
3PB Tests, 4PB Tests, Softening Localization, Material Properties, Epoxy Resin, Moment Curvature, Load Deflection, Digital Image Correlation Technique

Correspondence
M.Y. Fard,
Department of Mechanical and Aerospace Engineering,
School for Engineering of Matter, Transport and Energy,
Arizona State University,
Tempe,
AZ 85287-6106, USA
Email: masoud.yekanifard@asu.edu

Received: October 10, 2010;
accepted: July 12, 2013

doi:10.1111/ext.12050

Abstract

The effect of local strain and stress distribution in the polymeric material under out of plane loading is of interest in many applications. Flexural testing of the polymer resins is necessary to evaluate their mechanical behavior. In this paper, the flexural response of polymer resin Epon 863 mixed with the curing agent EPI-CURE 3290 using a 100/27 weight ratio has been investigated in three-point bending (3PB) and four-point bending (4PB) at different strain rates. Beams with different lengths and span to depth ratios were tested. Results show a higher flexural strength for 4PB than 3PB. Strain fields within the polymer beam structure were determined using the digital image correlation (DIC) technique to study the evolution of softening localization in 3PB and 4PB setups. Results show that the length of the softening localization is less than half of the thickness throughout the loading. The DIC technique was used to obtain the location of the neutral axis in the nonlinear stage of the material behavior. Results indicate the nonlinear variations of the neutral axis location for epoxy resin Epon E 863. The results show that the DIC technique can accurately characterize the material response of an epoxy resin for flexural loading.

Introduction

The mechanical properties of fiber-reinforced polymer composites are of increasing interest as their applications in mechanical and civil industries, such as aircraft-engine fan cases and concrete joints (anchoring steel bars to concrete), become widespread. These properties are dominated by those of the matrix, so the role of epoxy resin in polymer matrix composites is extremely important due to the nonlinear nature of polymer behavior. Mechanical properties of polymer resins should be characterized to provide a link between the macroscopic mechanical behavior of fiber-reinforced composites and microscopic mechanical behavior of their constituents. Conventional measurement tools used in mechanical tests include: surface-bonded resistive strain gages, extensometers, linear variable differential transducers (LVDTs), and actuators. Conventional measurements typically provide single measurements of strains and displacements at selected locations and gage lengths. The main issues associated with using conventional measurements are: (1) strain gage installation (e.g., surface preparation and misalignment) and stress concentrations; (2) need to remove extensometers from the specimen prior to failure to avoid damage in the instrument; (3) single point information; (4) transverse sensitivity of resistive strain gages; and (5) extra compliance of actuator system.

The digital image correlation (DIC) system is an optical noncontact and noninvasive method that employs tracking and image analysis for accurate two-dimensional (2D) and three-dimensional (3D) measurements of changes in the images. DIC was proven to be very effective at mapping deformation in mechanical testing.[1] Leendertz[2] developed the technique as an interferometric scheme involving photographic processing. The method has been demonstrated to be a sensitive tool for

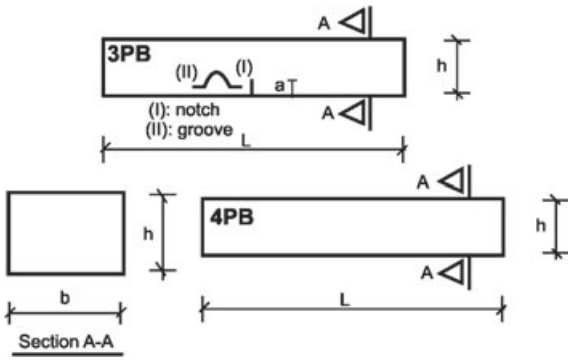

Figure 1 3PB and 4PB beam samples with rectangular cross sections.

Table 1 Average dimensions of bending samples

Sample No.	Initial imperfection	*b* (mm)	*h* (mm)	*a* (mm)	*L* (mm)	*S* (mm)	*S*/*h*
B-3PB-1 to B-3PB-2	Notch	10	4	1	60	50	12.5
B-3PB-3 to B-3PB-6	Groove			1.1			
B-3PB-7 to B-3PB-9	Notch	4	10	3	60	50	5
B-3PB-10 to B-3PB-12	Groove			3.2			
B-3PB-13 to B-3PB-15	Notch	12	4	1	90	78∗	19.5
B-3PB-16 to B-3PB-18	Groove			1.1			
B-3PB-19 to B-3PB-21	Notch	4	12	3	90	78∗	6.5
B-3PB-22 to B-3PB-24	Groove			3.2			
B-4PB-1 to B-4PB-10	—	4	10	—	60	50	5

∗ Span is 68mm in samples B-3PB-13 and B-3PB-19.

both in-plane and out-of-plane surface displacement measurements. For mechanical tests, the DIC system is widely used for full-field deformation measurement owing to the advantages of simple equipment, high precision, and noncontact measurement.[3–9] Two-dimensional DIC,[10] which is used with a single camera, can measure only in-plane displacement/strain fields on plane objects. Luo et al.[11] proposed a 3-D DIC technique, which combines DIC with stereo vision and can measure the 3-D displacement field. Chou et al.[12] studied the stress–strain compression behavior of polymethyl methacrylate (PMMA), cellulose acetate butyrate, polypropylene, and nylon 66 over a wide range of strain rates. The compressive yield behavior of two major monomers, Araldite MY721 and Araldite MY0510, were investigated as a function of temperature and strain rate.[13] Mannocci et al.[14] used three-point bending (3PB) tests to investigate the different environmental and aging effects on the mechanical properties of fiber posts. Fergusson et al.[15] used digital speckle photogrammetry technique to study the effect of defects on flexural behavior of sandwich composite structures. The DIC system was applied in a test program

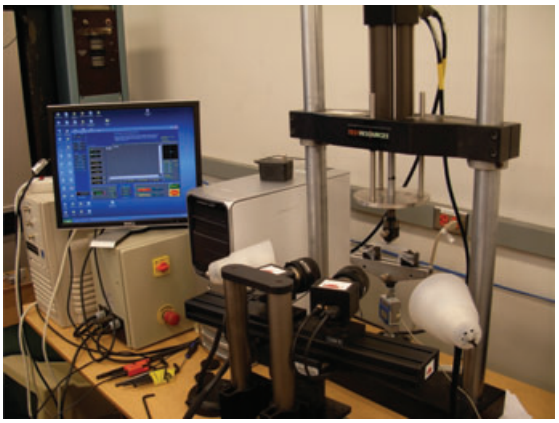

Figure 2 Equipment setup: electrical desktop machine, digital image correlation system cameras, 3PB fixture, and interface load cell.

Table 2 Plan of experimental monotonic bending tests

Sample No.	Longitudinal strain rate (μstr/s)	Span (mm)	Deflection measuring tool
B-3PB-1	59	50	Op, Ac
B-3PB-2	493	50	Op, Ac
B-3PB-3	65	50	Op, Ac
B-3PB-4 & B-3PB-5	164	50	Op, Ac
B-3PB-6	550	50	Op, Ac
B-3PB-7 & B-3PB-8	59	50	Op, Ac
B-3PB-9	493	50	Op, Ac
B-3PB-10	59	50	Op, Ac
B-3PB-11	493	50	Op, Ac
B-3PB-12	148	50	Op, Ac
B-3PB-13	26	68	Op, Ac
B-3PB-14	59	78	Op, Ac
B-3PB-15	493	78	Op, Ac
B-3PB-16	19	78	Op, Ac
B-3PB-17	65.8	78	Op, Ac
B-3PB-18	164	78	Op, Ac
B-3PB-19	78	68	Op, Ac
B-3PB-20 & B-3PB-21	59	78	Op, Ac
B-3PB-22	59	78	Op, Ac
B-3PB-23 & B-3PB-24	148	78	Op, Ac
B-4PB-1 to B-4PB-10	493	50	Op, Ac

Ac, actuator; Op, optical system.

to characterize the variability in woven roving E-glass/Vinyl ester composites.[16] The DIC system was successfully applied to study strain fields in specimens of solid wood, individual wood fibers, and papers,[17,18] as well as resin films,[19] fiber-reinforced polymer composites[20,21] and concrete.[22] Composite structures

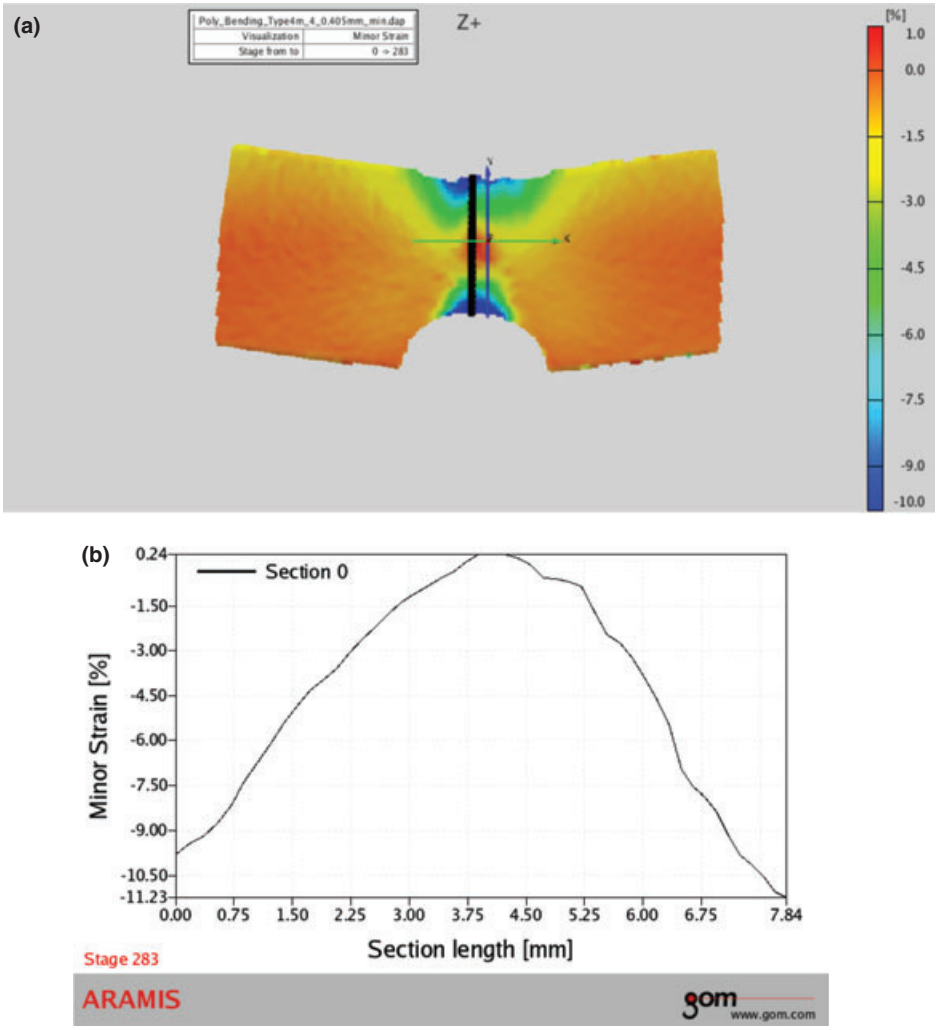

Figure 3 Stress concentration at the location of loading nose in sample B-3PB-22 before failure.

are usually subjected to large flexural loadings, so the flexural behavior of these structures and their constituents are critical to their use. Although there is a large body of literature on the mechanical and thermal properties of epoxy resins,[23−28] the properties of the same epoxy material can vary greatly with the curing agent.[29,30] The effect of the stress gradient in tensile and compressive peak stress and the entire stress–strain regime is important for any analytical or numerical study. A modified two-parameter Weibull model was used to compare the effect of loading systems on the mean stress in polymeric materials.[31] It was observed that the mean flexural strength is up to 40% higher than the mean tensile strength for a Weibull modulus greater than 14. Three-point bending (3PB) and four-point bending (4PB) tests are commonly used to evaluate the bending strength of metals, ceramics, and polymer materials. In this study, the loading techniques used are 3PB and 4PB, and the strength and ductility of the un-reinforced epoxy resin under flexure have been investigated. A notch or groove in the middle of the 3PB beams makes failure occur at the location of the initial notch or groove as the region around the notch or groove would be subjected to high stress values. This makes strain analysis of the central region by noncontact DIC technique much easier. As stated before, conventional methods such as strain gages for determining strain are not sufficient for evaluation of the strain field in bending samples as they provide information only at the location of strain gage. In addition, strain gages attached to the specimen might result in stress concentration and premature failure, so no information about post-peak response could be obtained. The DIC technique is used in this investigation as it is a reliable technique

Table 3 Mechanical characteristics for load deflection response of 3PB beam samples

Sample	Initial slope (N/mm)	Slope of post-LOP (N/mm)	MOR (MPa)	Δ_{MOR} (mm)	LOP (MPa)	Δ_{LOP} (mm)	Deflection at failure (mm)
B-3PB-1	57.49	n.a	n.a	n.a	87.2	1.90	2.45
B-3PB-2	60.00	n.a	n.a	n.a	n.a	n.a	1.77
B-3PB-3	45.22	18.31	117.66	3.6	96.5	2.38	4.26
B-3PB-4	45.62	n.a	n.a	n.a	97.77	2.39	3.01
B-3PB-5	47.56	18.90	118.5	3.99	92.7	2.4	4.24
B-3PB-6	48.11	21.99	120.13	3.94	90.3	2.34	4.12
B-3PB-7	219.93	115.04	100.3	1.54	73.9	0.92	1.67
B-3PB-8	224.09	90.7	106.08	1.69	81.4	0.96	2.44
B-3PB-9	230.8	96.6	111.9	1.72	83.3	0.94	2.16
B-3PB-10	199.4	70.3	121.2	2.63	76.04	0.97	3.46
B-3PB-11	202.05	76.9	132.2	2.7	83.3	1.05	3.14
B-3PB-12	201.6	68.8	124.7	2.67	80.8	1.03	3.27
B-3PB-13	20.3	n.a	n.a	n.a	n.a	n.a	4.4
B-3PB-14	18.83	n.a	n.a	n.a	n.a	n.a	4.89
B-3PB-15	19.46	n.a	n.a	n.a	n.a	n.a	3.86
B-3PB-16	17.2	12.07	115.44	6.41	93.44	4.83	6.41
B-3PB-17	17.44	12.42	116.6	6.88	90.03	4.84	7.17
B-3PB-18	18.27	13.2	110.46	6.6	88.9	4.67	6.6
B-3PB-19	141.2	79.7	91.96	2.7	61.02	1.47	3.01
B-3PB-20	135.7	n.a	n.a	n.a	63.7	1.34	2.61
B-3PB-21	141.19	n.a	n.a	n.a	65.3	1.29	2.29
B-3PB-22	112.5	44.8	111.6	4.24	70.4	1.75	5.72
B-3PB-23	120.0	n.a	n.a	n.a	n.a	n.a	2.07
B-3PB-24	127.2	79.4	125.71	3.39	81.4	1.73	3.78

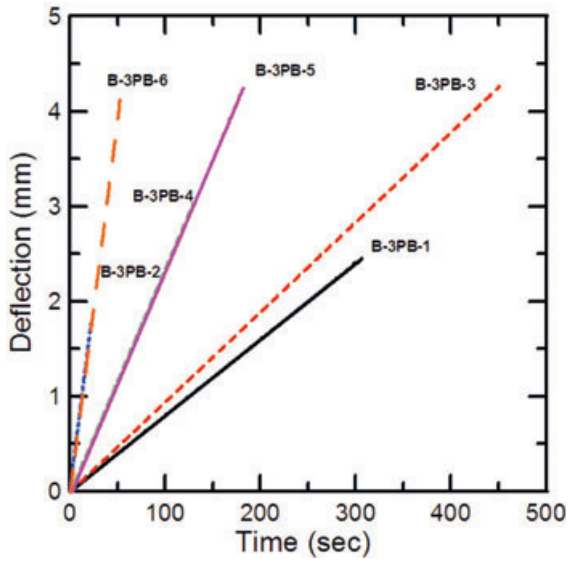

Figure 4 Deflection versus time for samples B-3PB-1 to B-3PB-6.

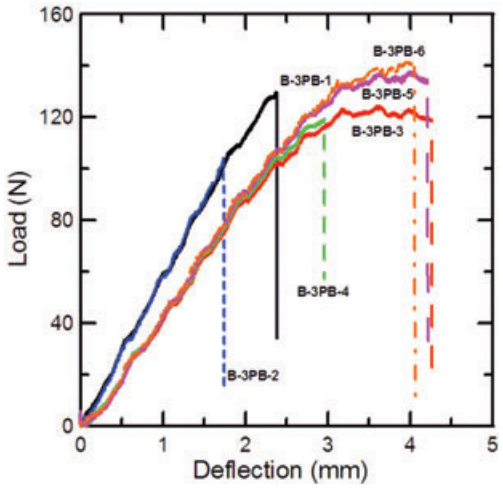

Figure 5 Load deflection curves of samples B-3PB-1 to B-3PB-6 under a monotonic 3PB test at different speeds at room temperature.

to determine the strain field across and along the sample especially in post-peak portion of the material behavior. The location of the neutral axis in 3PB setup is studied in the nonlinear phase of material behavior. The length of the softening localization at the location of the loading nose in 3PB and 4PB setups is examined using images taken with the DIC system. The results of this study will be used to investigate the stress–strain model for polymeric materials.

Flexural Samples

The materials used in this study were resin Epon 863 (Fiberglassite, MD, USA) with curing agent EPI-CURE

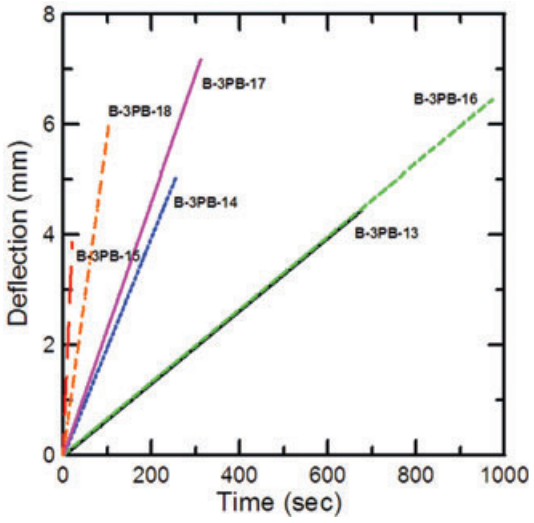

Figure 6 Deflection versus time for samples B-3PB-13 to B-3PB-18.

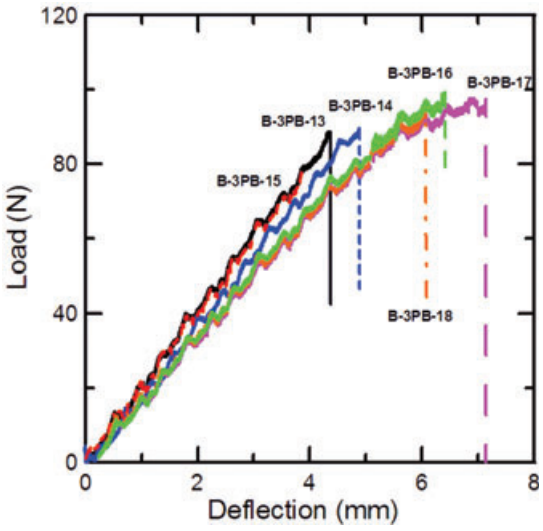

Figure 7 Load deflection curves of samples B-3PB-13 to B-3PB-18 under a monotonic 3PB test at different speeds at room temperature.

3290 (Fiberglassite, MD, USA) using a 100/27 weight ratio. ASTM standards D790[32] and D6272[33] were considered for bending samples. Beams with lengths of 60 and 90 mm were tested over a simply supported span of 50 and 78 mm, respectively. All the samples in 3PB setup initially had quarter deep notches in the middle of the beam, but half of the samples were modified by cutting out the material around the notch and making a groove. There is no notch or groove in the 4PB beams. The geometry and dimensions of the samples and the modified samples are shown in Fig. 1 and Table 1. The format of B-XPB-YY was used to name the specimens. X is 3 (for 3PB) or 4 (for 4PB) and YY is the serial number. L is the total length of the beam and S is the distance between the two supports. The spans allow enough space for the rotation of the beam at each support. The distance between a loading nose and the adjacent support in 4PB setup was 25 mm. A white base paint is sprayed on the face of the specimen to form a thin, uniform background. After the base color is dried, a speckle pattern of black is sprayed on the same face to form a random pattern covering approximately 50% of the face. The speckles should be of the same size as the speckles in the calibration plate used during calibration of the system.

Experimental Setup

Figure 2 shows the experimental setup in a 3PB test. An interface load cell was used to measure the axial load. All tests were conducted in displacement control and ambient environmental conditions. Deflection measurements were made using a DIC system. The loading rates corresponding to desired strain rates were calculated approximately based on the elastic linear assumption, type of a beam, and geometry of the samples. Equations (1) and (2) show the rate of loading for a 3PB beam with a groove or notch and a 4PB beam, respectively.

$$\frac{\mathrm{d}\delta}{\mathrm{d}t} = \frac{S^2}{6d}\frac{\mathrm{d}\epsilon}{\mathrm{d}t}\left(\frac{d_1}{d}\right)^2 \tag{1}$$

$$\frac{\mathrm{d}\delta}{\mathrm{d}t} = \frac{S_1\,(6S\text{-}7S_1)}{3d}\frac{\mathrm{d}\epsilon}{\mathrm{d}t} \tag{2}$$

where $\mathrm{d}\delta/\mathrm{d}t$ is the rate of loading, ϵ the axial strain, S the span, S_1 the distance between a loading nose and the adjacent support, d the thickness of the beam, and d_1 the thickness at the location of the groove or notch. Axial strain rates ranged from 26 to 550 μstr/s as shown in Table 2. The supporting and loading steel rods have a radius of 6.5 mm. The DIC system enables noncontact measurement of displacement and strain fields. Two digital cameras were used to capture the 3-D strain fields. A reference image has to be taken while the sample is unloaded, and all the images taken during the test will be referenced against the first image. The DIC system splits the images into correlated areas called facets. The transformation in facet size and shape is determined for every image. Post-processing software available within the system was used to determine the axial and shear strains in any given direction. The load–deformation relationship was found through the triggering option between the load cell and the system.

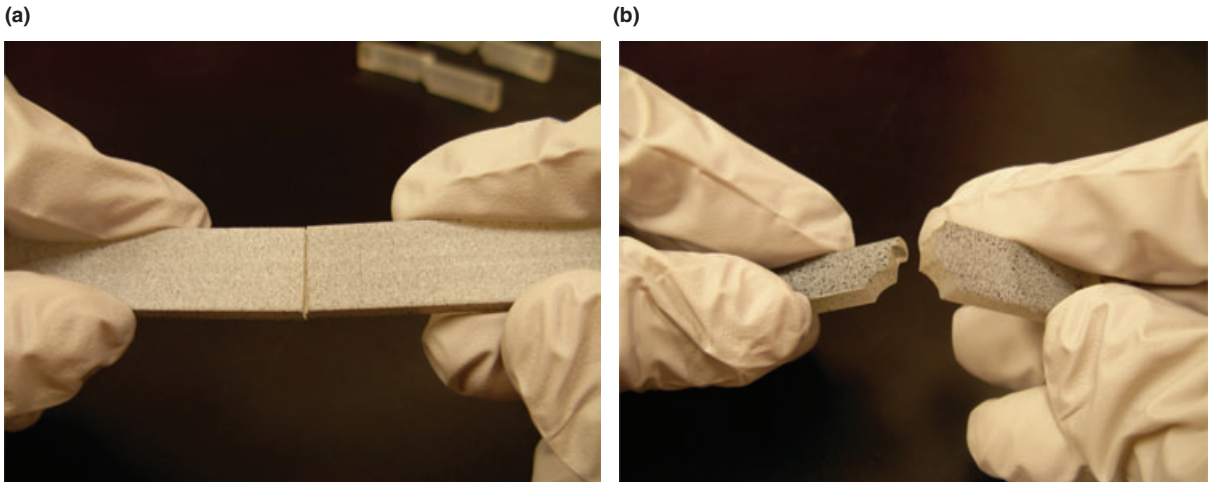

Figure 8 Fracture surface of the broken samples with notch and groove.

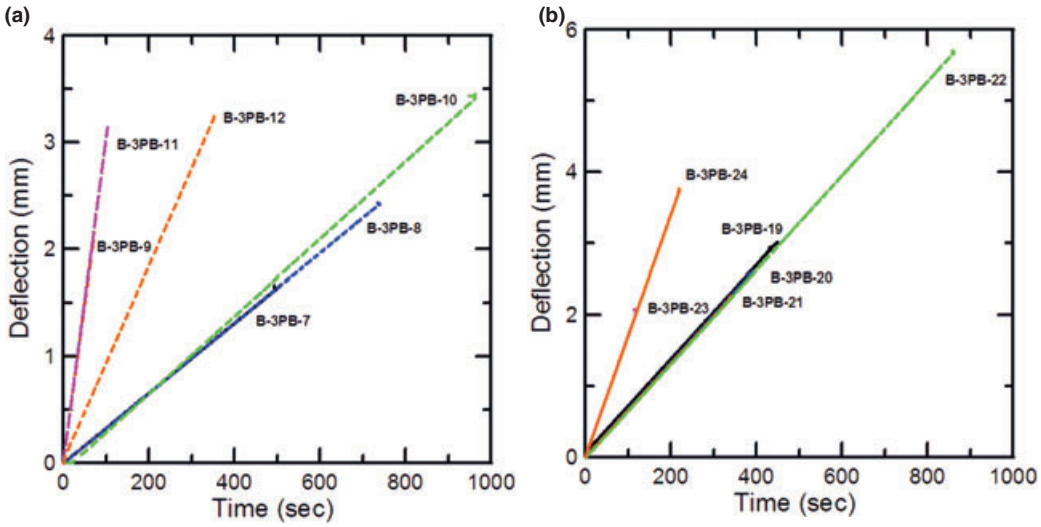

Figure 9 Deflection versus time for samples (a) B-3PB-7 to B-3PB-12 and (b) B-3PB-19 to B-3PB-24.

Results

Beam theory provides a relationship between shear force and the differential of the bending moment within the beam, as well as the relationship between axial stress and applied load.[34]

$$V = \frac{dM}{dx} \tag{3}$$

where V and M are shear force and bending moment, respectively. Changing the sign of shear stress at the mid-span could be confirmed by the results from the DIC technique. In 3PB, the shear force is constant in each half of the beam. The bending moment would rise linearly from zero at the supports to the maximum value at the location of the loading nose. In 4PB, there is no shear in the middle span of the beam and the moment is constant in the middle span. However, the region with stress concentration lies directly below the loading nose in both the setups as a result of the compression of the surface of the specimen by the loading nose. The stress concentration at the location of the loading nose in 3PB (B-3PB-22) is shown in Fig. 3. Figures 4 and 5 show the deflection versus time and the load deflection curves for samples B-3PB-1 to B-3PB-6 under a monotonic 3PB test at different load speeds at room temperature. While samples B-3PB-1 and B-3PB-2 with notch failed in the ascending part of the load deflection curve, samples B-3PB-3, B-3PB-5, and B-3PB-6 with groove failed after the peak point and at the start of deflection softening

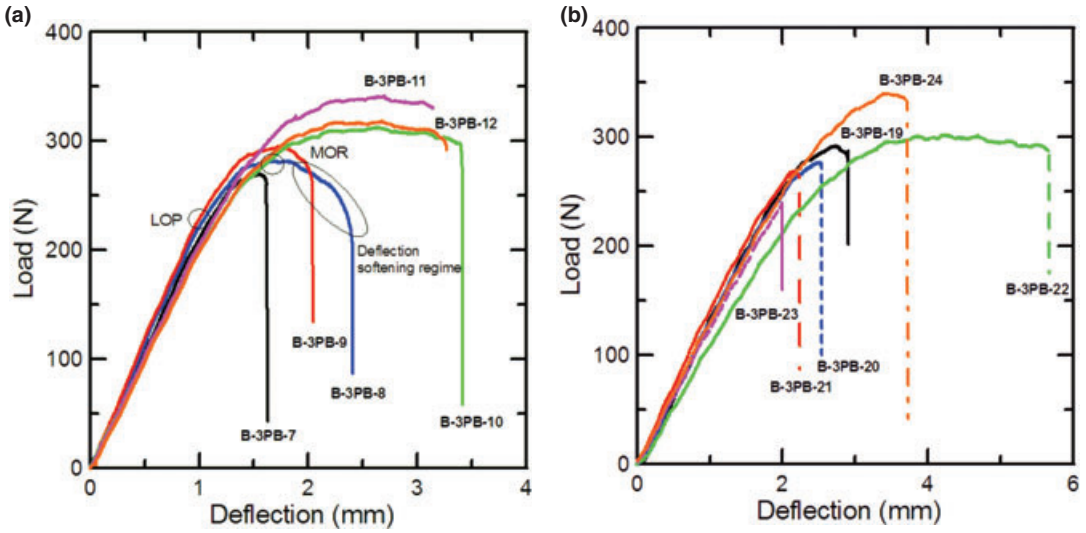

Figure 10 Load deflection curves under monotonic 3PB test at different speeds at room temperature (a) B-3PB-7 to B-3PB-12 and (b) B-3PB-19 to B-3PB-24.

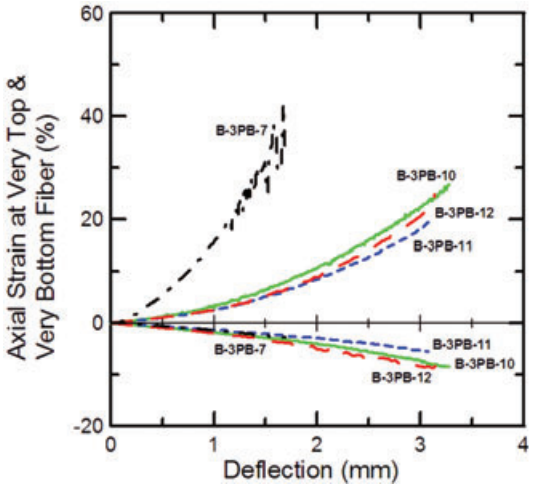

Figure 11 Axial strain distribution in top and bottom layer versus deflection at the middle of the beam for samples with notch and groove.

regime. By comparing the deflection time curves in Fig. 4, it is clear that samples B-3PB-2 and B-3PB-4 failed prematurely. The same trend has been observed for samples B-3PB-13 to B-3PB-18 as shown in Figs. 6 and 7. A possible cause for premature failure is the stress concentration at the location of the notch as fracture occurred along a straight line as shown in Fig. 8. Deflection at failure in notched samples is around 60% of the corresponding deflection failure in the grooved samples. Figures 9 and 10 show the deflection versus time and the load deflection curves for sample B-3PB-7 to B-3PB-12 and B-3PB-19 to B-3PB-24. The load initially increases proportionally to deflection in the elastic portion of the load deflection before passing through a knee point called the limit of proportionality (LOP). The LOP is defined as the point at which deviation is observed in the linear part of the stress–strain curve. The load keeps increasing with a reduced slope up to the maximum point known as the modulus of rupture (MOR), followed by a deflection softening regime and final failure. Deflection softening behavior in the flexural response indicates strain softening behavior of Epon E 863 in tension and compression. Brittle failure occurred after a considerable amount of plastic deformation in most of the samples. Mechanical characteristics of bending samples are summarized in Table 3.

Quantitative estimates of stress at the LOP point based on the MOR are presented in Table 3. The initial flexural stiffness was measured as the slope of the load deflection curve in the linear region between 0.3 and 1.00 mm. Samples with groove show a less initial stiffness than samples with notch even for the same load speed as observed from B-3PB-2, B-3PB-6, B-3PB-13, and B-3PB-16. Beams with higher thicknesses (10 mm) show more plastic deformation and less premature failure than the other samples because of less stress concentration effect around the sharp notch. This fact indicates that stress concentration plays a major role in the type of fracture and may overshadow the strain-rate effects on the MOR, degree of deflection softening, and the degree of nonlinearity in the material response. Results indicate that an increase in loading speed increases

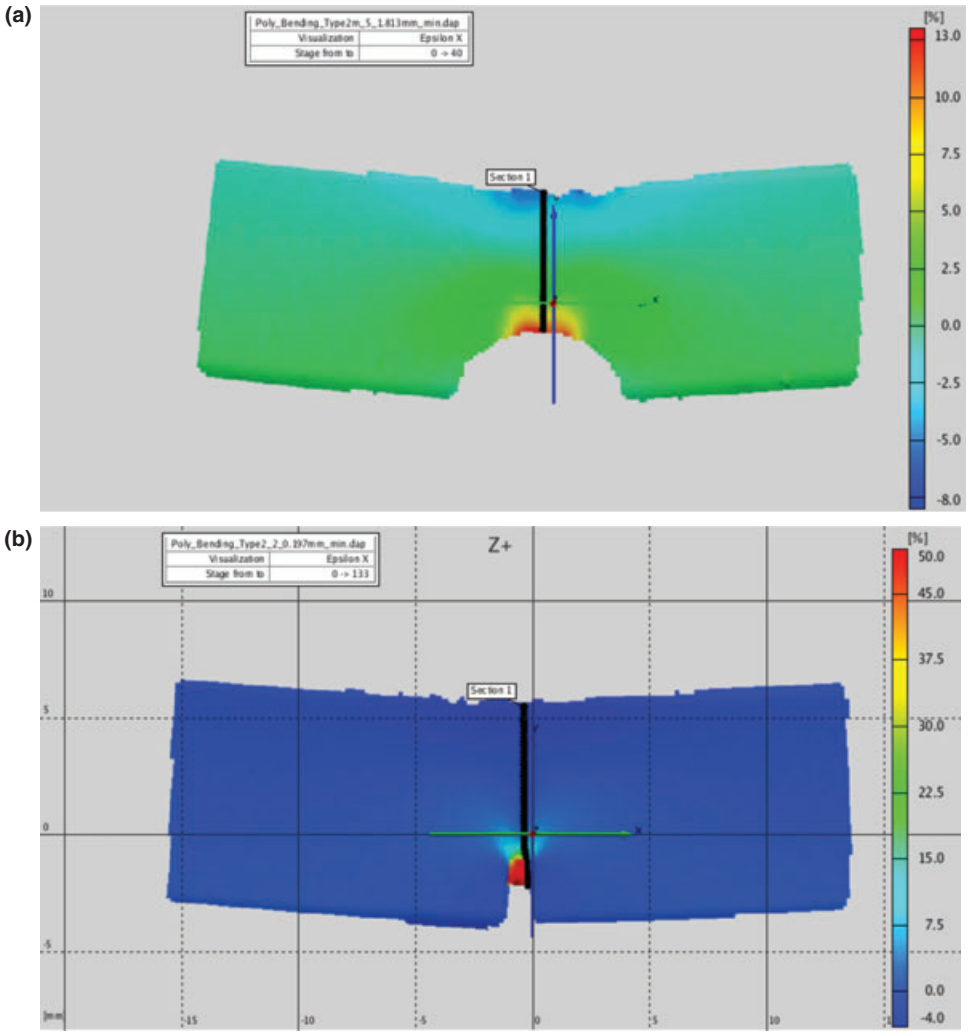

Figure 12 Effect of stress concentration on distribution of ϵ_x for samples with notch and groove.

the MOR and the initial bending stiffness in Epon E 863 (111.9 MPa in sample B-3PB-9 compared with 106.08 MPa for sample B-3PB-8). Figure 11 shows the strain at the very top and bottom fiber which was captured by the DIC system at the middle of the beam versus displacement at the mid-span. As the DIC system may not be able to resolve the very top and bottom surfaces during deformation, the strains observed by the DIC system were slightly less than the precise strains. Results show that increasing the strain in the top and bottom layers is more symmetric in beams with groove than in beams with notch because of the higher stress concentration effect in samples with notch. Figure 12(a) shows the slight effect of stress concentration on the axial strain field at the middle of the beam for B-3PB-11 with groove, while Fig. 12(b) illustrates the extreme effect of stress concentration due to the notch on axial strain distributions at the middle of beam B-3PB-8. The vertical strain distribution at the location of notch in B-3PB-8 is shown in Fig. 13. It is clear that higher thickness with a groove in the middle will increase the degree of nonlinearity and softening in the material behavior. Figure 14 clearly presents the nonlinearity in the moment curvature diagram and the effect of strain rate on the moment curvature response. Figure 15 shows the load deflection curves for the 4PB tests at 493 μstr/s. This figure also illustrates the average and the average-minus-one standard deviation load deflection curves for the 4PB results. Calculation of MOR for 3PB and 4PB based on linear elastic assumption shows that the MOR in 4PB is around 30% higher than the corresponding value in 3PB (171 MPa in 4PB compared with 132.5 MPa in 3PB).

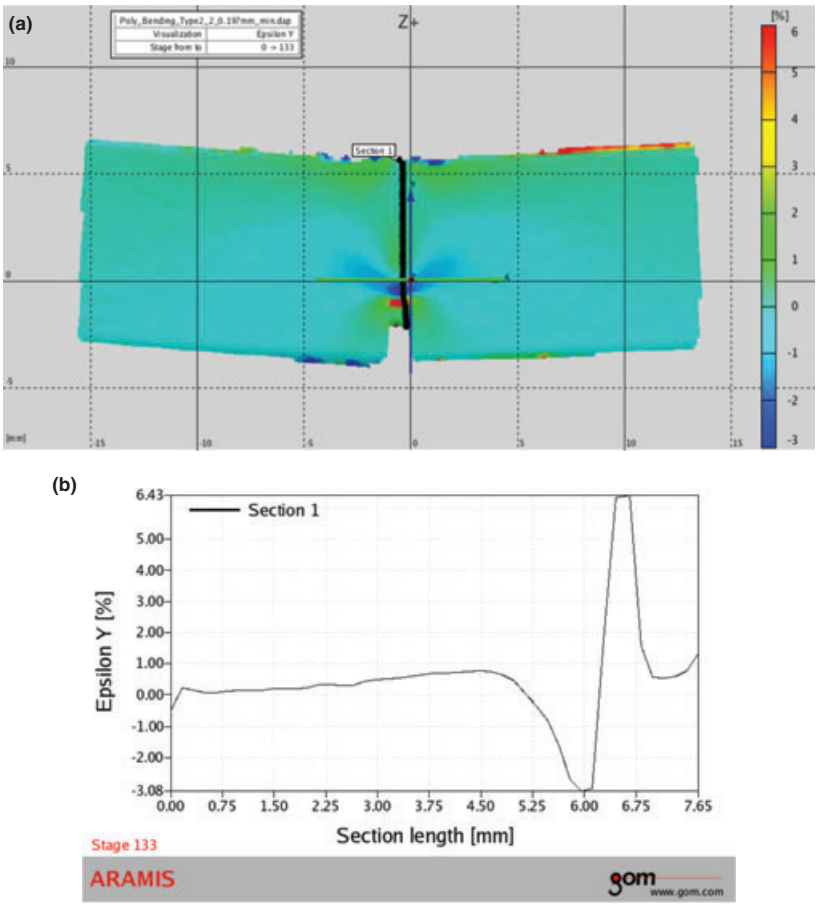

Figure 13 Effect of stress concentration due to notch on strain distribution ϵ_y in B-3PB-8.

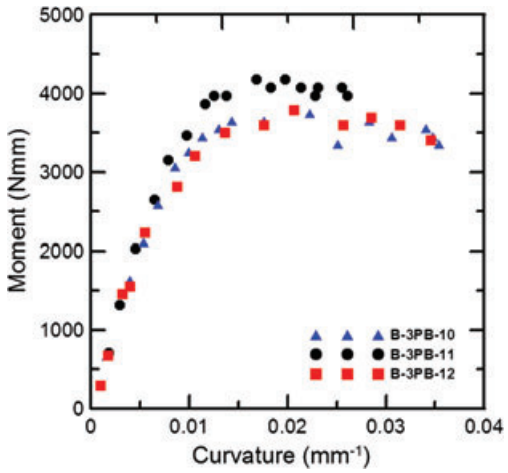

Figure 14 Moment curvature diagram in 3PB beams for different strain rates.

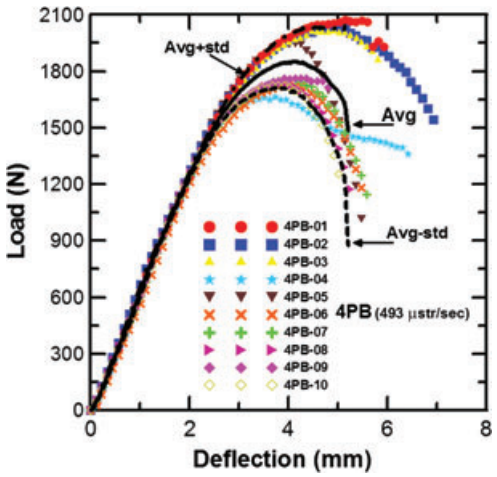

Figure 15 Load deflection curves in 4PB beams at 493 µstr/s.

The reason for a higher MOR in 4PB is that in 3PB with a groove at the center, the beam is forced to fracture at the location of groove. However, the center of the beam may not be the weakest point.

Location of Neutral Axis in Nonlinear Material Behavior

The location of the neutral axis during loading is an important parameter in the fracture mechanics study

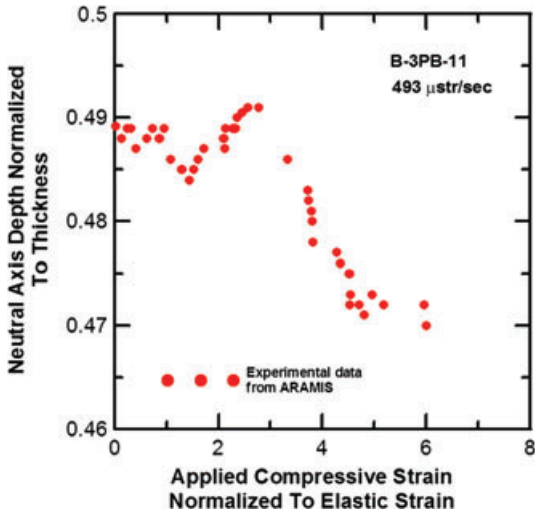

Figure 16 Location of the neutral axis throughout the loading.

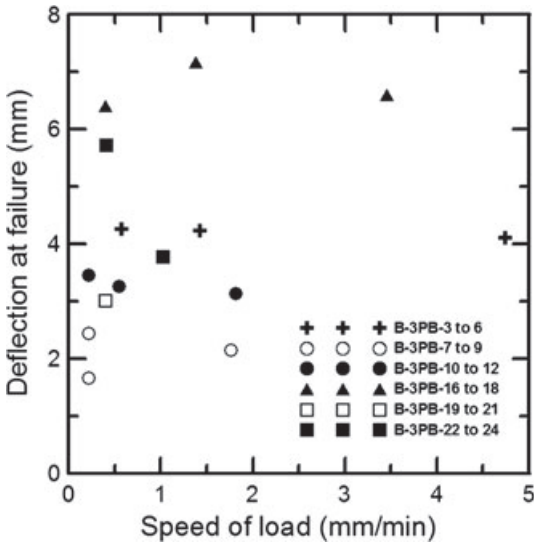

Figure 17 Variations of deflection at failure with rate of loading.

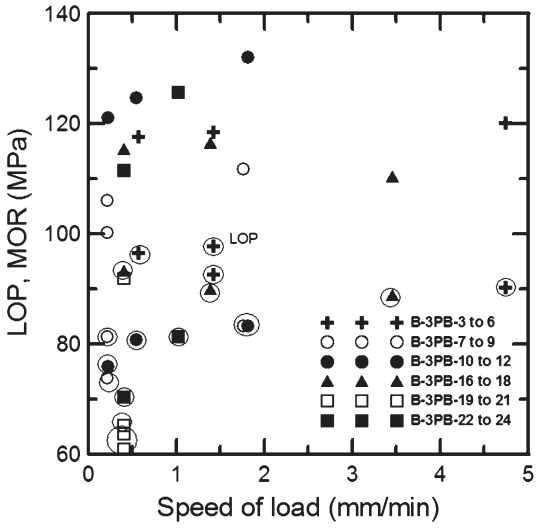

Figure 18 Variations of LOP and MOR with rate of loading (Note: symbols enclosed in circle indicate LOPs).

of a material. Figure 16 shows the location of the neutral axis normalized to thickness of the sample from the start of loading up to failure in the middle of the beam in the 3PB setup at 493 μstr/s, obtained from studying the stain field using the DIC system. Elastic strain obtained from the DIC system is 1.62%. These results imply that the location of the neutral axis directly depends on the tension and compression strengths in the nonlinear phase of pre-peak and post-peak material behavior.

Linear and Nonlinear Mechanical Properties

Bending specimens show a nonlinear material behavior and a considerable amount of plastic deformation. In this section, linear mechanical properties and the length of the softening localization in 3PB and 4PB are discussed. Figure 17 illustrates that there is no specific relationship between the deflection at failure and loading speed in the low speed rate domain. Results in Fig. 18 show that the MOR increases approximately linearly with increasing speed of loading except in samples B-3PB-16 to 18, where the increase in the MOR is followed by a decrease at 3.45 mm/min. This decrease might be due to the premature failure of sample B-3PB-18. Results show no specific trend in variation of LOP versus load speed.

Softening localization zone, which is a critical parameter to determine the amount of damping energy, was determined using the DIC system. Figure 19 shows the distribution of the longitudinal strain (ϵ_x) and the evolution of softening localization throughout the loading. Section lines in Fig. 19 show the location of the loading noses and the center of the beam. The marked areas around the loading noses show that plastic length is around 4.7 mm in 4PB beams. The fracture in some of the broken specimens occurred along the plane perpendicular to the direction of the maximum tensile stress on the tension side as shown in Fig. 8. It is to be noted that fracture usually occurs at the maximum principal tensile stress. Stress concentration has been observed around the loading nose in some of the samples. The effect of the stress concentration on the stress distribution has not been studied in this paper.

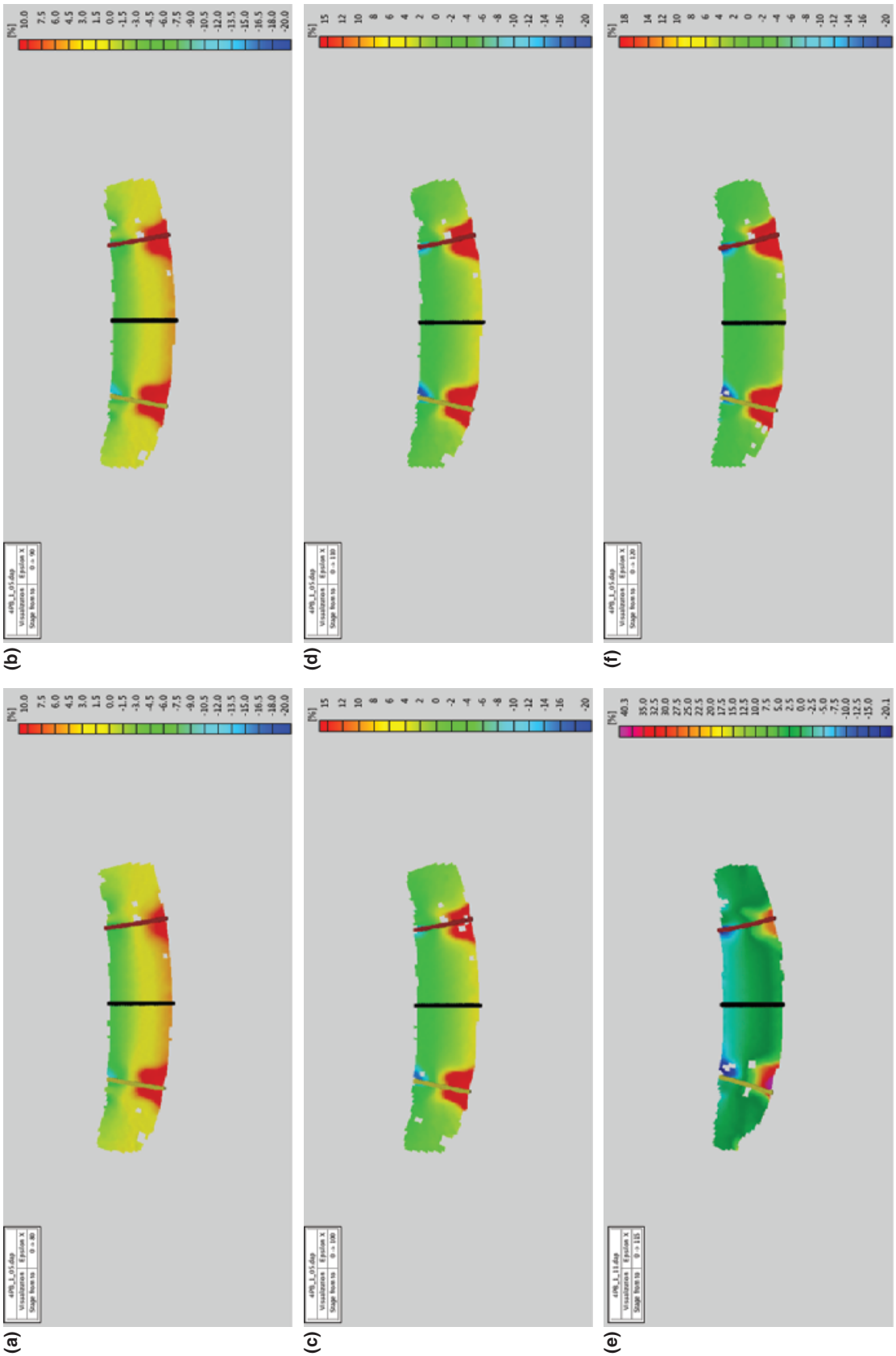

Figure 19 Evolution of softening localization in a 4PB beam.

Conclusion

In this study, the flexural linear and nonlinear responses of Epon 863 and curing agent EPI-CURE 3290 with a 100/27 weight ratio have been investigated in 3PB and 4PB setups at different strain rates using the DIC technique. The DIC system could accurately provide strain field information in the flexural tests for polymeric materials. The shear strains that were observed below the loading nose in 3PB were a result of stress concentration and the change in the sign of shear stress at the mid-span. Stress concentration due to the notch changes the strain distribution significantly in the beams, while the groove improves the stress concentration problem considerably. The DIC system is capable of determining the location of the neutral axis throughout the loading. Load deflection curves obtained from 3PB and 4PB tests show the deflection softening behavior of Epon E 863. Results showed that increasing the rate of loading increases the initial stiffness and MOR. Results also show the nonlinear nature of the moment curvature response and the effect of softening in the post-peak region. The length of the softening localization was measured throughout the loading and was less than half of the thickness. The moment curvature response obtained from the DIC system could be used as material data for nonlinear numerical simulations. Results show that the flexural strength for 4PB is higher than 3PB since in 3PB with a groove at the center, the beam is forced to fracture at the location of the groove. However, the center of the beam may not be the weakest point.

Acknowledgments

The authors gratefully acknowledge the support of this research by the Army Research Office, AMSRD-ARL-RO-SI Proposal Number: 49008-EG, Agreement Number: W911NF-07-1-0132, Program Manager: COL. Reed F. Young. We also thank Dr. Dallas Kingsbury from ASU for assistance in conducting the tests.

References

1. Archbold, E., Burch, J.M., and Ennos, A.E., ''Recording of in-Plane Surface Displacement by Double-Exposure Speckle Photography'', *Optica Acta* **17**: 883 (1970).
2. Leendertz, J.A., ''Interferometric Displacement Measurement on Scattering Surfaces Utilizing Speckle Effect'', *Journal of Physics* **3**: 214 (1970).
3. Chu, T., Ranson, W., and Sutton, M., ''Applications of Digital-Image Correlation Techniques to Experimental Mechanics'', *Experimental Mechanics* **25**(3): 232–244 (1985).
4. Sutton, M.A., Cheng, M., Peters, P.H., Chao, Y.J., and McNeill, S.R., ''Application of an Optimized Digital Correlation Method to Planar Deformation Analysis'', *Image Vision Computing* **4**(3): 143–150 (1986).
5. Schreier, H., Garcia, D., and Sutton, M., ''Advances in Light Microscope Stereo Vision'', *Experimental Mechanics* **44**(3): 278–288 (2004).
6. Helm, J.D., McNeill, S.R., and Sutton, M.A., ''Improved Three Dimensional Image Correlation for Surface Displacement Measurement'', *Optical Engineering* **35**(7): 1911–1920 (1996).
7. Helm, J.D., Sutton, M.A., and McNeill, S.R., ''Deformations in Wide, Center-Notched, Thin Panels, Part I: Three-Dimensional Shape and Deformation Measurements by Computer Vision'', *Optical Engineering* **42**(5): 1293–1305 (2003).
8. Sutton, M.A., Yan, J., Deng, X., Cheng, C.-S., and Zavattieri, P., ''Three Dimensional Digital Image Correlation to Quantify Deformation and Crack-Opening Displacement in Ductile Aluminum Under Mixed-Mode I/III Loading'', *Optical Engineering* **46**(5): 1–17 (2007).
9. Sutton, M.A., McNeill, S.R., Helm, J.D., and Chao, Y.J., ''Advances in Two-Dimensional and Three-Dimensional Computer Vision'', *PhotoMechanics* **77**: 323–372 (2000).
10. Pan, B., Qian, K.M., Xie, H.M., and Asundi, A., ''Two-Dimensional Digital Image Correlation for In-Plane Displacement and Strain Measurement: A Review'', *Measurement Science and Technology* **20**(6): 1–10 (2009).
11. Luo, P., Chao, Y., Sutton, M., and Peters, W., ''Accurate Measurement of Three-Dimensional Deformations in Deformable and Rigid Bodies Using Computer Vision'', *Experimental Mechanics* **33**(2): 123–132 (1993).
12. Chou, S.C., and Robertson, K.D., ''The Effect of Strain Rate and Heat Developed During Deformation on the Stress-Strain Curve of Plastics'', *Experimental Mechanics* **13**: 422–432 (1973).
13. Behzadi, S., and Jones, F.R., ''Yield Behavior of Model Epoxy Matrices for Fiber Reinforced Composites: Effect of Strain Rate and Temperature'', *Journal of Macromolecular Science Part B: Physics* **44**: 993–1005 (2005).
14. Mannocci, F., Sherriff, M., and Watson, T.F., ''Three-Point Bending Test of Fiber Posts'', *Journal of Endodontics* **27**: 758–761 (2001).
15. Fergusson, A.D., Puri, A., Morris, A., and Dear, J.P., ''Flexural Testing of Composite Sandwich Structures With Digital Speckle Photogrammetry'', *Applied Mechanics and Materials* **5-6**: 135–144 (2006).

16. Lopez-Anido, R., El-Chiti, F.W., Muszynnski, L., Dagher, H.J., Thompson, L.D., and Hess, P.E., *Composite Material Testing Using a 3-D Digital Image Correlation System*, *COMPOSITES 2004 Convention and Trade Show American Composites Manufacturers Association*, Tampa, FL (2004).
17. Mott, L., Shaler, S.M., and Groom, L.H., ''A Novel Technique to Measure Strain Distributions in Single Wood Fibers'', *Wood and Fiber Science* **28**(4): 429–437 (1996).
18. Muszyñski, L., Lagana, R., and Shaler, SM., ''Optical Measurements of Wood Deformations in Changing Climate,'' *2002 SEM IX International Congress on Experimental Mechanics*. Milwaukee, WI, pp. 298–301 (2002).
19. Muszyñski, L., Wang, F., and Shaler, S.M., ''Short Term Creep Tests on Phenol Resorcinol Formaldehyde (PRF) Resin Undergoing Moisture Content Changes'', *Wood and Fiber Science* **34**(4): 612–624 (2002).
20. Muszyñski, L., Lopez-Anido, R., and Shaler, SM., ''Image Correlation Analysis Applied to Measurement of Shear Strains in Laminated Composites,'' *The SEM IX International Congress on Experimental Mechanics*. Orando, FL, pp. 163–166, (2000).
21. Melrose, P., Lopez-Anido, R., and Muszyñski, L., ''Elastic Properties of Sandwich Composite Panels Using 3-D digital Image Correlation With the Hydromat Test System,'' *SEM XI International Congress and Exposition on Experimental and Applied Mechanics*. Costa Mesa, CA, p. 490 (2004).
22. Choi, S., and Shah, S.P., ''Measurement of Deformations on Concrete Subjected to Compression Using Image Correlation'', *Experimental Mechanics* **37**(3): 307–313 (1997).
23. Buckley, C.P., and Harding, J., ''Deformation of Thermosetting Resins at Impact Rates of Strain, Part I: Experimental Study'', *Journal of the Mechanics and Physics of Solids* **49**(7): 1517–1538 (2001).
24. Buckley, C.P., and Dooling, P.J., ''Deformation of Thermosetting Resins at Impact Rates of Strain, Part 2: Constitutive Model With Rejuvenation'', *Journal of the Mechanics and Physics of Solids* **52**(10): 2355–2377 (2004).
25. Khan, M.Z.S., and Simpson, G., ''A Comparison of the Mechanical Properties in Compression of Two Resin Systems'', *Materials Letters* **52**(3): 173–179 (2002).
26. Gilat, A., Goldberg, R.K., and Roberts, G.D., ''Strain Rate Sensitivity of Epoxy Resin in Tensile and Shear Loading'', *Journal of Aerospace Engineering, ASCE* **20**(2): 75–89 (2007).
27. Jordan, J.L., Foley, J.R., and Siviour, C.R., ''Mechanical Properties of Epon 826/DEA Epoxy'', *Mechanics of Time-Dependent Materials* **12**: 249–272 (2008).
28. Littell, J.D., Ruggeri, C.R., Goldberg, R.K., Roberts, G.D., Arnold, W.A., and Binienda, W.K., ''Measurement of Epoxy Resin Tension, Compression, and Shear Stress-Strain Curves Over a Wide Range of Strain Rates Using Small Test Specimens'', *Journal of Aerospace Engineering, ASCE* **21**: 162–173 (2008).
29. Kozey, V. and Kumar, S., ''Compressive Behavior of Epoxy Resins,'' *International SAMPE Technical Conference*, (1994).
30. Miwa, M., and Takeno, A., ''Strain Rate and Temperature Dependence of Shear Properties of Epoxy Resin'', *Journal of Materials Science* **30**(7): 1760–1765 (1995).
31. Giannotti, M.I., Galante, M.J., Oyanguren, P.A., and Vallo, C.I., ''Role of Intrinsic Flaws Upon Flexural Behavior of a Thermoplastic Modified Epoxy Resin'', *Polymer Testing* **22**: 429–437 (2003).
32. ASTM D790. ''Standard Test Method for Flexural Properties of Unreinforced and Reinforced Plastics and Electrical Insulatins Materials,'' (2003).
33. ASTM D6272. ''Standard Test Method for Flexural Properties of Unreinforced and Reinforced Plastics and Electrical Insulating Materials by Four-Point Bending,'' (2002).
34. Timoshenko, S.P., and Gere, J.M., *Mechanical of Materials*, 3rd Edition, *PWS-KENT Publishing Company*, MA, USA (2004).